ELSEVIER

Physics of the Earth and Planetary Interiors 98 (1996) 17–29

PHYSICS OF THE EARTH AND PLANETARY INTERIORS

Quasi-harmonic computations of thermodynamic parameters of olivines at high-pressure and high-temperature. A comparison with experiment data

François Guyot [a,*], Yanbin Wang [a], Philippe Gillet [b,1], Yanick Ricard [b]

[a] *Center of High Pressure Research, Dept. ESS, University at Stony Brook, Stony Brook, NY 11794-2100, USA*
[b] *Laboratoire de Sciences de la Terre (URA CNRS 726), ENS Lyon, 46, allée d'Italie, 69364 Lyon cedex 07, France*

Received 15 September 1995; revised 19 December 1995; accepted 2 January 1996

Abstract

Specific volumes of forsterite and San Carlos olivine have been measured by in-situ X-ray diffraction at simultaneously high pressure and high temperature up to 7 GPa and 1300 K in a cubic-anvil press coupled to synchrotron radiation. No difference could be evidenced between the thermal pressure of the two compounds. It has been shown that the parameter αK_T is volume-independent within the volume range investigated in this study for both forsterite and San Carlos olivine. A quasi-harmonic calculation of the high-pressure high-temperature specific volumes of forsterite has been performed and shown to be in good agreement with the experimental results. Then, a self consistent model of all the thermodynamic functions of forsterite was constructed, the input consisting of the experimental ultrasonic and vibrational spectroscopic data exclusively. The model accurately reproduces not only the experimental P–V–T data measured in this study, but also the high-temperature, 1 bar thermal expansion, the adiabatic incompressibility, the constant pressure specific heat and the entropy measurements, without using other a priori information.

1. Introduction

Olivine is the major mineral of peridotite and is therefore believed to be one of the most abundant phases in the Earth's upper mantle. Accurate determination of its molar volume (or density) at high-pressure and temperature is of great importance to compare laboratory measurements with seismic models, as well as to assess thermodynamic properties of olivine at any point of its stability field. However, such molar volumes have not yet been systematically measured at simultaneous high pressures and temperatures relevant to the upper mantle of the Earth, although measurements by Meng et al. (1993) are available on the pure magnesium endmember at about 7 GPa and temperatures between 1000 K and 1400 K.

In the present study, we have performed in-situ X-ray diffraction measurements at pressures up to 7 GPa and temperatures between 298 K and 1200 K on pure synthetic forsterite and San Carlos olivine with

* Corresponding author at: Laboratoire de Minéralogie–Cristallographie (URA CNRS 09) and Institut de Physique du Globe de Paris, Tour 16, Case 115, 4, place Jussieu, 75252 Paris cedex 05, France.

[1] Fellow of the Institut Universitaire de France.

PII S0031-9201(96)03174-3

Fe/(Fe + Mg) = 0.098(3). High-pressure high-temperature volumes of forsterite obtained from these experiments are compared with calculations based on experimental vibrational density of states derived from spectroscopic data (ultrasonic, Raman and infrared). Additionally, these models allow calculations of thermal expansions, high-temperature incompressibilities and entropies, making comparisons with 1 bar measurements and subsequent extrapolations in the pressure–temperature field possible. Data and calculations lead to an internally consistent thermochemical data set for forsterite. Apart from being geophysically important, forsterite serves as a useful test model compound for which both microscopic and macroscopic parameters are available with reasonable precision.

2. Experimental details

Synthetic forsterite (Mg_2SiO_4) fine-grained powder identical to that described in Gwanmesia and Liebermann (1992) and natural San Carlos olivine of Fe/(Fe + Mg) ratio of 0.098(3), checked by electron microprobe were used as starting materials.

High pressures were generated by a cubic-anvil press apparatus (SAM-85), described by Weidner et al. (1992), using tungsten carbide anvils with 4×4 mm^2 square truncations. The pressure medium was a 6 mm edge length cube made of a mixture of boron powder and epoxy resin (wt ratio 4–1) cold compressed at about 75 MPa. A cylindrical hole (3 mm in diameter) was drilled in the cube so as to accommodate an amorphous carbon sleeve, used as a heating element and a boron nitride sleeve used as sample container. Details of the cell assembly are shown in Fig. 1. During the experiments, heating of the sample was provided to the cell assembly by a d.c. power supply delivering an adjustable constant power input.

Temperatures were measured with a $W_{0.95}Re_{0.05} - W_{0.74}Re_{0.26}$ thermocouple. The power supply provided temperatures stable within 5 K or less (measured from the fluctuations of the thermocouple reading). Diffraction data were collected as close as possible to the thermocouple hot junction. Temperature variations within the diffracting volume have been estimated to be less than 5 K (Wang et al., 1994). No pressure correction was applied to the thermocouple reading. At the maximum pressure reached in this study, this effect should not exceed a few K (see for example Ohtani et al., 1982, p. 261).

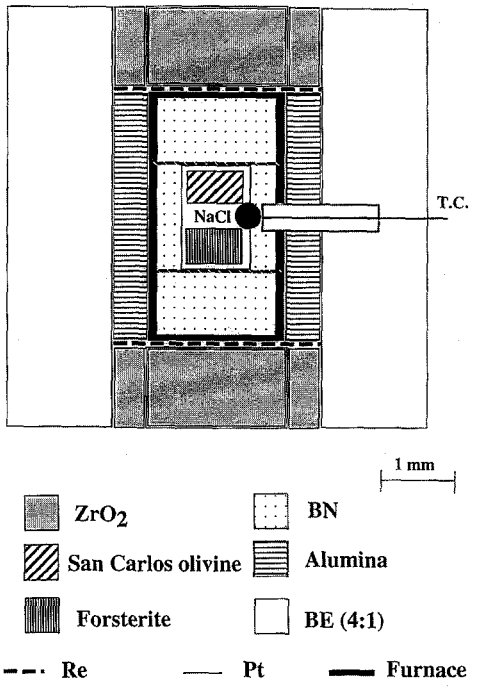

Fig. 1. Cell assembly used for this study in SAM-85. ZrO_2, Zirconia endplugs; BN, Boron nitride sleeve; BE (4:1), Boron epoxy; Re, Rhenium disc; Pt, platinum wire. Diffraction spectra were collected close to the thermocouple hot junction in order to reduce the effect of temperature gradients.

The white X-ray beam was provided by the superconducting wiggler beamline (X17B1) at National Synchrotron Light Source (NSLS) at Brookhaven National Laboratory, New York, USA. Energy-dispersive X-ray diffraction data were collected at a fixed scattering angle of $2\theta = 7.5°$ with a solid-state germanium detector. The incident X-ray beam was collimated with slits of 100×200 μm^2 (horizontal–vertical) used to restrict the diffracting volume in the cell assembly. The diffracted beam was collimated by a collimator (100 μm vertical) and slits of 100×300 μm^2 (horizontal–vertical) restricting the 2θ acceptance angle within $+/-$ 0.01°. The diffraction parallelogram in the sample had therefore approximately the following characteristics: 100×750 μm^2 and 7.5° angle. A volume of

about 0.002 mm^3 corresponding to 10 μg of sample was thus analysed. The relation between channel number and d-spacing, characteristic of the multichannel analyser and of the diffraction geometry, was calibrated at the beginning and at the end of the experiment with both the characteristic fluorescence lines of molybdenum and lead, as well as with the positions of main diffraction peaks in a mixture of Si, Al_2O_3 and MgO. The 1 bar patterns of the NaCl pressure calibrant and of the forsterite sample before and after the run provided additional cross checks. Standard fluctuations or driftings of the calibration have been reported to affect d-spacing measurements by less than 0.0005–0.0008 Å in a single run (Wang et al., 1994).

A NaCl–BN powder mixture was loaded together with the samples, NaCl being used as a pressure calibrant valid at high-temperature, and BN for slowing down the recrystallisation process of the heated rocksalt. Five diffraction lines: 111, 200, 220, 222 and 420, were generally used for determining the NaCl molar volume by a least squares fitting procedure. The P–V–T equation of state of Decker (1971) was used to determine the pressure, given the measured volume and the temperature thermocouple reading. A detailed discussion of the uncertainty in this pressure calibration is given in Meng et al. (1993). It is concluded that, in the case of hydrostatic conditions, the total error, including uncertainty in cell parameter measurements as well as systematic errors in the P–V–T equation of state of NaCl, will not exceed 0.16 GPa.

3. Results

3.1. Non-hydrostatic stresses

Non-hydrostatic effects are one of the main causes of systematic errors during equation of state measurements in high-pressure vessels and, therefore, need to be dealt with as accurately as possible in order to remove low quality data points from the final data set. The differential stress in the high-pressure cell has been calculated for each data point (see Table 1) by a method based on the NaCl diffraction line shifts (Weidner et al., 1992). Here non-hydrostatic stress is expressed as $(\sigma_1 - \sigma_3)$, where σ_1 and σ_3 are the axial (vertical) and radial (horizontal) stress components, respectively (Weidner et al., 1992). It is difficult to give an error bar for the stress values given in Table 1 because such uncertainties are a complex combination of errors in the positions of the diffraction lines, as well as errors in the elastic constants of NaCl (especially at high temperatures

Table 1
Pressure, temperature and differential stress for all the data points sorted in chronological order of acquisition. Pressure and deviatoric stress are measured from diffraction patterns in sodium chloride

Data	P (GPa)	T (°C)	Differential stress (GPa)
1	0.00	25	0.00
2	0.73	25	0.22
3	1.88	25	0.20
4	2.40	25	0.24
5	4.42	25	0.10
6	4.39	202	0.11
7	4.45	402	0.02
8	4.34	595	0.00
9	4.26	750	−0.03
10	4.10	700	−0.03
11	4.03	648	−0.03
12	3.98	596	−0.08
13	3.78	498	−0.05
14	3.57	398	−0.04
15	3.21	200	−0.02
16	2.96	25	−0.03
17	3.53	25	−0.06
18	3.93	25	−0.10
19	4.32	25	−0.12
20	4.71	25	−0.07
21	5.10	25	−0.15
22	5.48	25	−0.18
23	5.85	25	−0.16
24	6.36	401	−0.04
25	6.94	799	−0.02
26	7.01	897	−0.01
27	7.05	999	0.05
28	6.49	699	0.02
29	6.22	498	−0.01
30	5.76	299	0.07
31	5.24	25	0.11
32	4.84	25	0.15
33	4.12	25	0.07
34	3.18	25	0.14
35	3.97	603	0.05
36	3.45	399	−0.03
37	2.78	25	0.03
38	0.00	25	0.00

and pressures). Taking into account all these uncertainties, errors as large as 20% of the values of the stresses might be possible. Non-hydrostaticity strongly depends on the pressure–temperature history of the sample. In our experiment, the stress history of the cell can be accurately followed in Table 1. First, compression at room temperature leads to strong non-hydrostatic conditions (data 2–5) due to high yield strength (~ 0.2 GPa) of NaCl; the yield strength decreases markedly with increasing temperature releasing non-hydrostatic stress (data 6–9). On cooling, the state of low deviatoric stress is generally preserved (data 10–16). A second room temperature compression of the sample again leads to non-hydrostatic states (data 17–23) and the stress is released by the second heating–cooling cycle (data 24–30). The room temperature decompression then leads to rather high deviatoric stresses (data 31–34) which are partially annealed by a short heating–cooling event (data 35–36) before terminating data acquisition. The non-systematic behaviour of the sign of deviatoric stress (e.g. upon compression or decompression) illustrates the complexity of mechani-

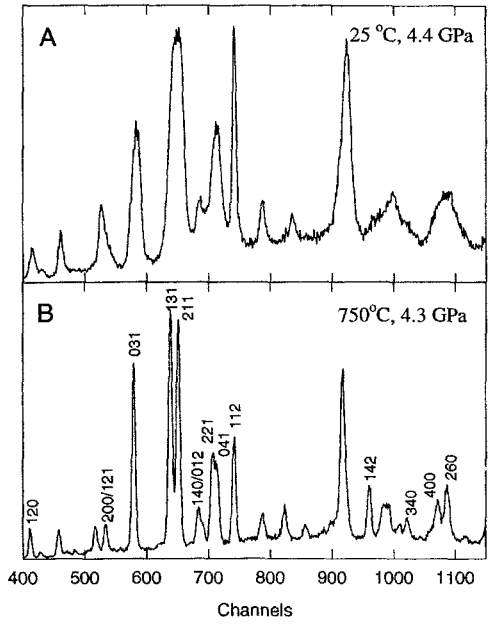

Fig. 2. Effect of the non-hydrostatic stress on the diffraction linewidths in olivine. (A) Spectrum of San Carlos olivine corresponding to data #6 acquired after room temperature compression to 4.39 GPa; (B) spectrum of San Carlos olivine at 4.26 GPa and 750°C corresponding to data #9 and acquired after heating the olivine displayed in (A). The sharpening of the diffraction peaks with increasing temperature is obvious from the figure. Only diffraction peaks used for unit-cell refinments have been indexed in the figure. Other peaks are olivine peaks not used in the refinment and one boron nitride peak coming from the boron nitride sleeve.

Table 2
Refinements of unit cell parameters in forsterite and San Carlos olivine corresponding to data 26 (7.01 GPa and 897°C)

hkl	drefined	dexperimental	Difference	Difference (%)
Forsterite				
120	3.8357	3.8389	−0.0032	−0.08
101	3.6964	3.6975	−0.0011	−0.03
200	2.9744	2.9686	0.0058	0.19
031	2.7359	2.7356	0.0003	0.01
131	2.4848	2.4846	0.0002	0.01
211	2.4382	2.4389	−0.0007	−0.03
221	2.2483	2.2488	−0.0005	−0.02
041	2.2221	2.2210	0.0011	0.05
222	1.7347	1.7353	−0.0006	−0.03
142	1.6548	1.6542	0.0006	0.04
400	1.4842	1.4843	−0.0001	−0.01
260	1.4600	1.4604	−0.0004	−0.03
San Carlos olivine				
120	3.8436	3.8497	−0.0061	−0.16
101	3.7002	3.7037	−0.0035	−0.09
200	2.9779	2.9772	0.0007	0.02
031	2.7429	2.7415	0.0014	0.05
131	2.4899	2.4903	−0.0004	−0.02
211	2.4436	2.4446	−0.0010	−0.05
140	2.3203	2.3232	−0.0029	−0.12
221	2.2535	2.2543	−0.0008	−0.04
041	2.2276	2.2262	0.0014	0.06
311	1.8016	1.8008	0.0008	0.04
222	1.7380	1.7385	−0.0005	−0.03
142	1.6579	1.6574	0.0005	0.03
340	1.5609	1.5600	0.0009	0.06
400	1.4883	1.4886	−0.0003	−0.02
260	1.4645	1.4645	0.0000	0.00

Forsterite: $a = 5.93725$ Å error = 0.00183 (0.06%); $b = 10.06455$ Å error = 0.00388 (0.08%); $c = 4.72574$ Å error = 0.00283 (0.12%); $V = 282.39$ Å^3 error = 0.1515 (0.11%).
San Carlos olivine: $a = 5.95432$ Å error = 0.00160 (0.05%); $b = 10.09263$ Å error = 0.00346 (0.07%); $c = 4.73020$ Å error = 0.00279 (0.12%); $V = 284.2602$ Å^3 error = 0.1521 (0.11%).
drefine: refined values of the parameters.
dexperimental: measured values of the parameters.
hkl are the Miller indices of the crystallographic planes.

cal processes at work in this particular cell. As seen from Table 1, non-hydrostatic stresses generally vanish once the cell assembly has been heated above 600°C, but of course, this really represents non-hydrostaticity in the sodium chloride and not in the sample. The linewidth in the sample diffraction patterns is a sensitive indicator of the state of local non-hydrostatic stress, i.e. that varies from point to point (Fig. 2). It is impossible to get meaningful data from spectra such as that of Fig. 2(A). Therefore, in the following, only data which correspond to low levels of stress measured in sodium chloride as well as diffraction patterns in olivines with linewidths similar or thinner than in the 1-bar spectrum are kept.

Table 3
Unit-cell parameters and volumes of forsterite. See Table 1 for P, T and differential stress associated to each data point. No data were collected at points 2, 4, 17, 18, 20, 21 and 22

Data	V (Å^3)	a (Å)	b (Å)	c (Å)	Error V (Å^3)
1	289.7100	5.9823	10.1920	4.7518	0.0926
3	286.2463	5.9774	10.1784	4.7049	0.7036
5	280.2278	5.8908	10.0037	4.7553	0.6767
6	282.6359	5.9210	10.0454	4.7519	0.6266
7	283.7480	5.9359	10.0663	4.7487	0.3016
8	285.7589	5.9554	10.1128	4.7448	0.1830
9	287.2217	5.9677	10.1375	4.7477	0.0915
10	286.9784	5.9643	10.1332	4.7483	0.1107
11	286.4753	5.9621	10.1278	4.7443	0.1056
12	286.2082	5.9602	10.1234	4.7434	0.1098
13	285.7515	5.9545	10.1176	4.7431	0.1079
14	285.3204	5.9531	10.1102	4.7405	0.1395
15	284.0636	5.9432	10.0953	4.7345	0.0695
16	283.4631	5.9389	10.0873	4.7317	0.0972
19	280.1822	5.9193	10.0521	4.7088	0.1609
23	277.2358	5.9060	10.0113	4.6888	0.2620
24	278.4870	5.9149	10.0276	4.6952	0.2588
25	281.7171	5.9270	10.0482	4.7303	0.1313
26	282.3900	5.9373	10.0646	4.7257	0.1515
27	283.7871	5.9440	10.0772	4.7378	0.1305
28	281.6907	5.9306	10.0566	4.7231	0.1451
29	280.9777	5.9239	10.0460	4.7214	0.1569
30	279.9579	5.9181	10.0409	4.7113	0.1578
31	278.7294	5.9093	10.0259	4.7046	0.1078
32	279.7298	5.9157	10.0370	4.7112	0.1527
33	281.9676	5.9267	10.0586	4.7298	0.1053
34	283.6867	5.9399	10.0898	4.7335	0.0734
35	287.0792	5.9657	10.1326	4.7493	0.0621
36	286.1257	5.9572	10.1176	4.7472	0.0674
37	284.4529	5.9454	10.1006	4.7367	0.1037
38	289.7100	5.9841	10.1807	4.7554	0.1029

Table 4
Unit-cell parameters and volumes of San Carlos olivine. See Table 1 for P, T and deviatoric stress associated to each data point. No data were collected at points 2, 4, 17, 18, 20, 21 and 22

Data	V (Å^3)	a (Å)	b (Å)	c (Å)	Error V (Å^3)
1	291.9225	5.9916	10.2287	4.7632	0.1188
3	288.8497	5.9692	10.1723	4.7570	0.4868
5	284.9442	5.9824	10.0654	4.7321	1.5327
6	285.5929	5.9680	10.0941	4.7408	1.6328
7	286.8112	5.9485	10.1355	4.7571	1.2988
8	288.0155	5.9762	10.1472	4.7495	0.1720
9	289.3220	5.9836	10.1688	4.7549	0.1068
10	289.0887	5.9812	10.1663	4.7542	0.0750
11	288.8123	5.9738	10.1621	4.7539	0.1158
12	288.5352	5.9761	10.1575	4.7533	0.0982
13	288.0770	5.9729	10.1528	4.7505	0.1083
14	287.7289	5.9704	10.1476	4.7492	0.1165
15	286.6930	5.9630	10.1367	4.7430	0.1082
16	286.1568	5.9569	10.1310	4.7417	0.1153
19	283.3177	5.9405	10.0936	4.7250	0.1110
23	279.7014	5.9214	10.0457	4.7021	0.2560
24	280.8315	5.9299	10.0584	4.7084	0.2082
25	283.2358	5.9466	10.0848	4.7229	0.1535
26	284.2602	5.9543	10.0926	4.7302	0.1521
27	285.6822	5.9593	10.1034	4.7448	0.0952
28	284.0922	5.9486	10.0874	4.7344	0.1363
29	283.2934	5.9406	10.0792	4.7313	0.1690
30	282.1858	5.9358	10.0726	4.7197	0.1475
31	281.4420	5.9259	10.0605	4.7208	0.1221
32	282.2302	5.9344	10.0724	4.7216	0.1240
33	284.5280	5.9448	10.0985	4.7395	0.1099
34	286.5699	5.9606	10.1285	4.7467	0.0875
35	289.1702	5.9809	10.1612	4.7582	0.0782
36	288.3222	5.9736	10.1513	4.7546	0.0713
37	286.9030	5.9621	10.1375	4.7469	0.0589
38	291.7044	5.9998	10.2142	4.7599	0.1083

3.2. Sample unit-cell volumes

Unit-cell volumes of both forsterite and San Carlos olivine were determined from 12 to 16 diffraction lines by least squares fitting. Representative average refinements of the cell parameters of the two compounds are shown in Table 2. The stability of the results has been tested and confirmed by changing the number and the indices of the diffraction lines

Table 5
Thermal pressure (in GPa) in forsterite (ΔPthfor1 and ΔPthfor2) and in San Carlos olivine (ΔPthSanca)

T (K)	Data	ΔPthfor1 [a]	ΔPthfor2 [b]	ΔPthSanca
300	1	−0.1	0.0	0.0
675	7	1.6	1.7	2.0
868	8	2.4	2.5	2.5
1023	9	3.0	3.1	3.1
973	10	2.8	2.9	2.8
921	11	2.4	2.5	2.6
869	12	2.3	2.4	2.4
771	13	1.9	2.0	2.0
671	14	1.4	1.5	1.6
473	15	0.5	0.6	0.8
300	16	−0.1	0.0	0.2
1072	25	3.0	3.1	2.7
1170	26	3.4	3.5	3.3
1272	27	4.2	4.3	4.1
972	28	2.5	2.7	2.7
771	29	1.9	2.0	2.0
572	30	0.9	1.0	0.9
300	38	−0.1	0.0	−0.1

[a] Obtained using $V_0 = 289.92$ Å^3.
[b] Obtained using $V_0 = 289.72$ Å^3.

involved in the refinement. For example, if the 140, 311 and 340 are used to refine the forsterite data of Table 2, the measured volume changes by less than 0.03% whereas the deviation to the fit increases to 0.19%. Note that if spectra showing stress-induced line broadening are refined, the error bars in volume jump by a factor of 10 (see for instance data 2 to 7 in Tables 3 and 4). The unit cell parameters and volumes of forsterite and San Carlos olivine are given in Tables 3 and 4.

4. Discussion

4.1. Thermal pressure in forsterite and San Carlos olivine

As seen in Table 1, room temperature data points were generally affected by relatively large levels of non-hydrostatic stresses and will thus not be used further. The high-temperature high-pressure data are of better quality, and it is interesting to discuss them within the theoretical framework of thermal pressure. The thermal pressure is obtained by subtracting the pressure at volume V and at room temperature,

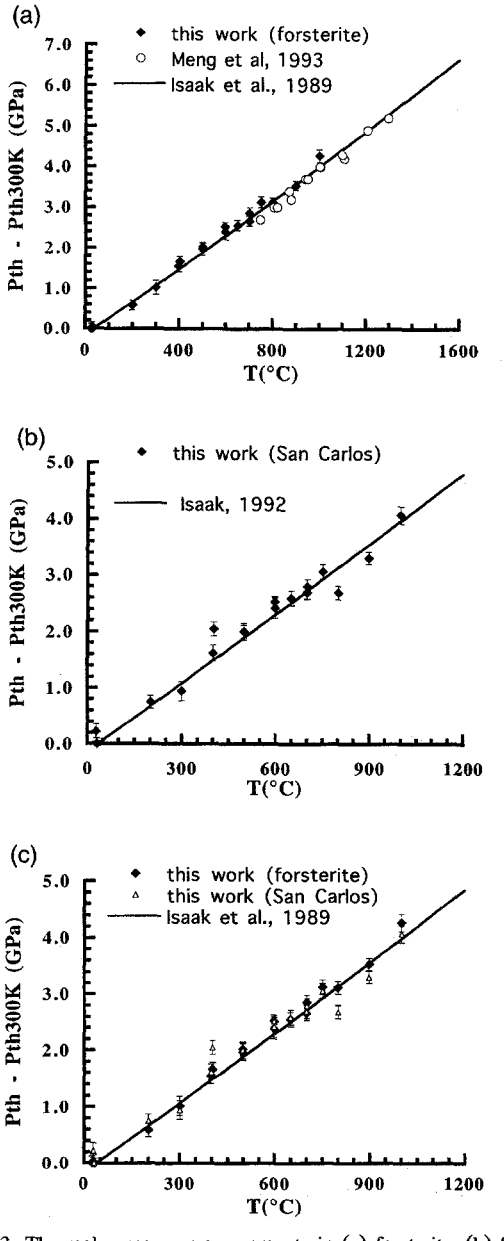

Fig. 3. Thermal pressure measurements in (a) forsterite, (b) San Carlos olivine, (c) both compounds, compared with measurements inferred from ultrasonic data by Isaak et al. (1989) and Isaak (1992).

obtained from a third order Birch–Murnaghan equation of state:

$$P = \frac{3}{2}K_0\left[\left(\frac{V_0}{V}\right)^{\frac{7}{3}} - \left(\frac{V_0}{V}\right)^{\frac{5}{3}}\right] \times\left[1 + \frac{3}{4}(K_0' - 4)\left(\left(\frac{V_0}{V}\right)^{\frac{2}{3}} - 1\right)\right] \quad (1)$$

from the pressure measured at the same V and at temperature T. The parameters K_0, K_0' and V_0 correspond to the values of isothermal bulk modulus, pressure derivative of isothermal bulk modulus and volume, respectively, all at 300 K and 1 bar. More exactly, this procedure gives the difference ΔP_{th} between thermal pressure at T and thermal pressure at room temperature:

$$\Delta P_{th} = P_{th}(T,V) - P_{th}(300\,K,V) = P(T,V) - P(300\,K,V) \quad (2)$$

In forsterite, thermal pressures ΔP_{th} were calculated using Eq. (1) and Eq. (2) with $K_0 = 127.4$ GPa (Isaak et al., 1989), $K_0' = 4.8$ (Graham and Barsch, 1969), and $V_0 = 289.72$ Å^3 (our data point at 1 bar). Using $V_0 = 289.92$ Å^3 (Schwab and Küstner, 1977) slightly shifts the thermal pressures to lower values, by an amount similar to the experimental error bar (Table 5). In San Carlos olivine, thermal pressures at room temperature were calculated in the same way assuming $K_0 = 130$ GPa (inferred from Isaak, 1992), $K_0' = 5.13$ (Kumazawa and Anderson, 1969), and using our V_0 value. The results are listed in Table 5 and plotted in Fig. 3. The larger scatter of the data observed in San Carlos olivine (Fig. 3(b)) is probably due to minor chemical destabilisation of Fe^{2+} at high temperatures in the cell assembly, but it is clear that no significant difference in thermal pressure can be evidenced between forsterite and San Carlos olivine (Fig. 3(c)). The difference in data quality between forsterite and San Carlos olivine, however, suggests that precise P–V–T measurements at high-temperatures are more difficult on iron-bearing silicates than on iron-free phases.

As shown in Fig. 3(a), our thermal pressure measurements in forsterite agree very well with the higher temperature measurements by Meng et al. (1993) using the same experimental method. The measurements in forsterite and San Carlos olivine also agree with thermal pressure calculations of Isaak et al. (1989) and Isaak (1992). The fact that the experimental data of the present work and of Meng et al. (1993) follow the thermal pressure lines from the Isaak et al. (1989) and Isaak (1992) results implies that αK_T is volume independent for olivine within the volume range provided by the present synchrotron data. This was predicted by O.L. Anderson (e.g. Anderson, 1984, 1995; Anderson et al., 1992).

5. Quasi-harmonic calculations of high-pressure high-temperature volumes

In order to better understand the behaviour of minerals under extreme conditions, it is important to relate the thermal pressure to other thermodynamic properties such as entropies, as well as to vibrational properties. Forsterite is an ideal case to test such consistency since both macroscopic and microscopic data have been precisely measured at least within some pressure–temperature range, and as far as thermal equations of states are concerned, computations can be compared directly with the thermal pressure measurements in forsterite discussed above. Since both microscopic and macroscopic data are more scarce for San Carlos olivine, the present discussion will be restricted to forsterite. Calculations can be easily performed with a classical model of statistical thermodynamics giving the quasi-harmonic vibrational free energy including a simple anharmonic correction (e.g. Wallace, 1972) as:

$$F_{th} = \int\left(\left[\frac{h\nu}{2} + kT\ln\left(1 - \exp\left(-\frac{h\nu}{kT}\right)\right) + ak_BT^2\right]g(\nu)\,d\nu \quad (3)$$

where the integration runs over the vibrational density of states $g(\nu)$, ν is the vibrational frequency, h and k_B are the Planck and Boltzman constants, respectively, and the parameter a is an anharmonic term (also frequency-dependent) which can be identified to the anharmonic parameter defined by (e.g. Gillet et al., 1991):

$$a(\nu) = \left(\frac{\partial \ln \nu}{\partial T}\right)_v \quad (4)$$

Then, since $P = -(\partial F/\partial V)_T$, we have

$$P_{th} = \int \left(\frac{\gamma}{V} \left[\frac{h\nu}{2} + \frac{h\nu}{\exp\frac{h\nu}{k_B T} - 1} \right] - \frac{mak_B T^2}{V} \right) g(\nu)\mathrm{d}\nu \quad (5)$$

where γ is the mode Grüneisen parameter (frequency-dependent) and m a second anharmonic parameter defined as:

$$m(\nu) = \left(\frac{\partial \ln a}{\partial \mathrm{Ln} V} \right)_T \quad (6)$$

The mode Grüneisen parameter $\gamma(\upsilon)$ is volume-dependent through Eq. (7), defining the parameter $q(\upsilon)$:

$$q = (\partial \ln \gamma / \partial \mathrm{Ln} V)_T \quad (7)$$

The high-pressure high-temperature volumes are obtained by solving:

$$P(T,V) = \frac{3}{2} K_0 \left[\left(\frac{V_0}{V} \right)^{\frac{7}{3}} - \left(\frac{V_0}{V} \right)^{\frac{5}{3}} \right] \times \left[1 + \frac{3}{4}(K_0' - 4) \left(\left(\frac{V_0}{V} \right)^{\frac{2}{3}} - 1 \right) \right] + P_{th}(T,V) - P_{th}(300\,\mathrm{K}, V) \quad (8)$$

Finally, the consistency with entropy measurements can be tested by applying:

$$S = \int \left[-k_B \mathrm{Ln} \left(1 - \exp\left(\frac{-h\nu}{k_B T} \right) \right) + \frac{h\nu}{T\left(\exp\left(\frac{h\nu}{k_B T} \right) - 1 \right)} - 2ak_B T \right] g(\upsilon)\mathrm{d}(\upsilon) \quad (9)$$

with the same notations as in Eq. (3).

For solving Eq. (5), Eq. (8) and Eq. (9) in the case of forsterite, we used $K_0 = 127.4$ GPa (Isaak et al., 1989), $K_0' = 4.8$ (Graham and Barsch, 1969) and $V_0 = 43.67$ cm^3 mol^{-1}. The anharmonic parameter m was taken equal to 0 since neither experimental measurements nor theoretical estimates are available. In this approximation, a non-zero value for the anharmonic contribution only appears in the expression for entropy (Eq. (9)); the anharmonic terms do not contribute to the equation of state (Eq. (5) and Eq. (8)). This quasi-harmonic approximation might be a

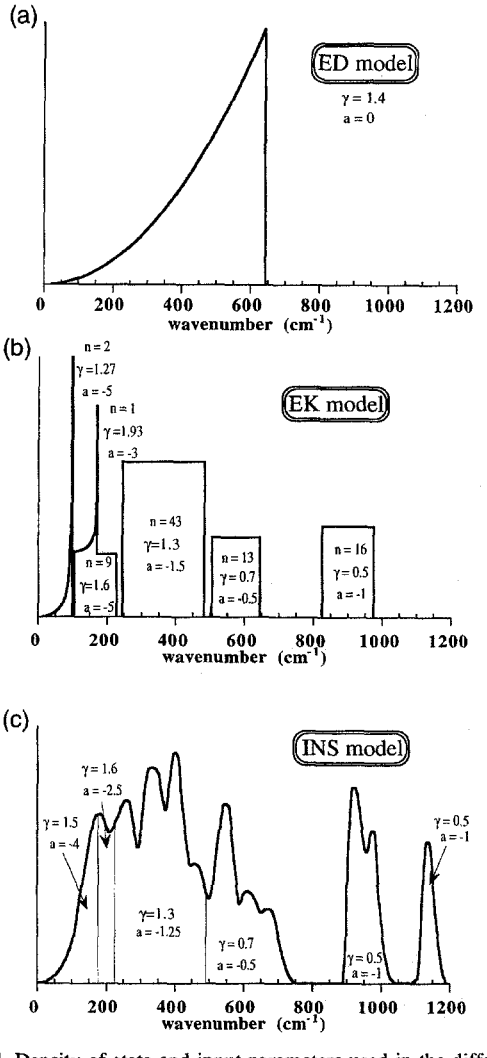

Fig. 4. Density of state and input parameters used in the different models (a) extended Debye (ED) model; (b) extended Kieffer (EK) model; (c) inelastic neutron scattering (INS) model. In each case, the anharmonic parameters "a" and Grüneisen parameter γ are specified. In the EK model, the number n of oscillator per vibrational box is also given.

problem only at temperatures higher than the experimental range investigated here. Several vibrational models were used to estimate the vibrational density of state:

1. An extended Debye model (Ita and Stixrude, 1992, and Fig. 4(a)) where $g(\upsilon)$ is a classical Debye function (see e.g. Kieffer, 1979a,b) and γ is frequency-independent (Ita and Stixrude, 1992). In this model, (hereafter designated ED-model) input parameters are the Debye temperature (θ_d = 924 K), the Grüneisen parameter at $V = V_0$ (γ = 1.14), and the q parameter ($q = 1$), all taken from Ita and Stixrude (1992). No anharmonic term ($a = 0$) is taken into account.
2. An extended Kieffer's model (Kieffer, 1979, Kieffer, 1980, see Fig. 4(b)) based on model 1 of Gillet et al. (1991), and hereafter designated EK-model. For acoustic modes, the Grüneisen parameters are calculated from ultrasonic data by Graham and Barsch (1969). The mode Grüneisen parameters have been measured for 20 Raman modes (Chopelas, 1990) and 16 infra-red modes (Hofmeister et al., 1989). These data have been used directly to ascribe values of the Grüneisen parameters for different frequency ranges of the density of state (Fig. 4(b)). Almost no measurements of the evolution of the Grüneisen parameters with volume (i.e. of the mode q parameters) have been performed in forsterite. Because of the small number of measurements and of their large uncertainties, we have assumed the mode Grüneisen parameters to have constant q parameters with a value identical to that used in the extended Debye model (i.e. $q = 1$). This approximation might be crude and further experimental measurements of q parameters are needed. Values of the anharmonic parameters "a" for different ranges of the density of state are taken from the model of Gillet et al. (1991) and incorporated in the calculations of entropies and specific heats.
3. A model (INS-model) based on existing inelastic neutron scattering data (Rao et al., 1988, and Fig. 4(c)). The Grüneisen parameters and anharmonic parameters used in the model for the different ranges of the density of state are given in Fig. 4(c). The attributions are made in a similar way as in the EK-model. Although the origin and existence of vibrational energy above 1100 cm^{-1} are not well established, we decided not to deviate from the model of Rao et al. (1988). For these modes, we used the Grüneisen parameters and anharmonic parameters, experimentally constrained for the high-frequency modes in the 900–1000 cm^{-1} range.

Table 6
Experimental results vs model calculations (extended Debye and spectroscopic models) for molar volume of forsterite at high-pressure and high-temperature

Data[a]	T (K)	P (GPa)	Vexp	V_{ED}	V_{EK}	V_{INS}
	675	4.45	42.72	42.69	42.70	42.67
a	868	4.32	43.02	42.97	42.98	42.95
a	1023	4.26	43.24	43.22	43.20	43.16
a	973	4.10	43.20	43.20	43.19	43.15
a	921	4.03	43.13	43.15	43.14	43.11
a	869	3.98	43.09	43.09	43.09	43.06
a	771	3.78	43.02	43.02	43.03	43.00
a	671	3.57	42.95	42.96	42.97	42.94
a	473	3.21	42.77	42.82	42.84	42.82
a	1072	6.94	42.41	42.46	42.44	42.41
a	1170	7.01	42.51	42.56	42.54	42.50
a	1272	7.05	42.72	42.69	42.67	42.61
a	972	6.49	42.41	42.46	42.46	42.42
a	771	6.22	42.30	42.29	42.30	42.27
b	1019	7.6	42.14	42.20	42.19	42.16
b	1077	7.4	42.29	42.33	42.32	42.28
b	1144	7.3	42.43	42.44	42.44	42.39
b	1213	7.2	42.57	42.56	42.54	42.50
b	1278	7.2	42.66	42.65	42.63	42.58
b	1380	7.0	42.79	42.85	42.83	42.76
b	1478	7.1	42.96	42.95	42.93	42.86
b	1569	7.0	43.08	43.11	43.08	43.00
b	1093.3	7.3	42.33	42.38	42.36	42.33
b	1151.1	7.0	42.46	42.54	42.53	42.48
b	1222.3	6.9	42.66	42.67	42.65	42.60
b	1274.4	6.9	42.76	42.73	42.72	42.66
b	1371.2	6.6	42.94	42.96	42.93	42.88

[a] Measurements this work.
[b] Measurements Meng et al. (1993).

The different models give good results within the range of experimental volume measurements (Table 6): all the models reproduce the experimental values of molar volume within 0.2%. The INS-model gives slightly smaller volumes than the others at temperatures between 1000 K and 2000 K. This is probably due to the presence of vibrational energy at high frequency, around 1100 cm^{-1}, which remains unsaturated at such temperatures. The spectroscopic models (EK and INS) are more consistent with the entropy at any temperature than the ED-model (Fig.

5(a)). The inability of Debye models to predict entropies in orthosilicates had already been pointed out by Kieffer (1979b) and is largely due to the inaccuracy of Debye density of states when applied to complex minerals. Constant-pressure specific heat is reasonably well predicted by the three models, although discrepancies of about 2% can exist (Fig. 5(b)). Such discrepancies are probably due to the anharmonic terms which are either imprecisely estimated (EK and INS models) or not taken into account (ED-model). This latter point explains why the ED-model underestimates Cp at 2000 K by about 3%. Another important test is to compare the models with 1-bar thermal expansion measurements (Fig. 6(a)). Not surprisingly, the ED-model is in very good agreement with the experimental measurements of Kajioshi (1986) since these specific thermal expansion data have been used for the fitting procedure (Ita and Stixrude, 1992). The spectroscopic models (EK and INS), which do not contain such a priori

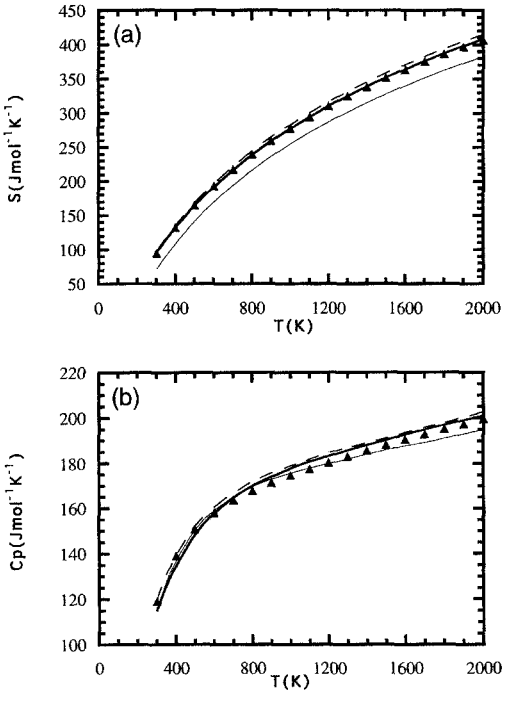

Fig. 5. Comparison of experimental results and model calculations at 1 bar and high temperature for (a) entropy, (b) constant pressure specific heat. Solid triangles: experimental data taken from Saxena et al. (1993) and Gillet et al. (1991). Thick solid line, INS model; thin solid line, ED model; dashed line, EK model.

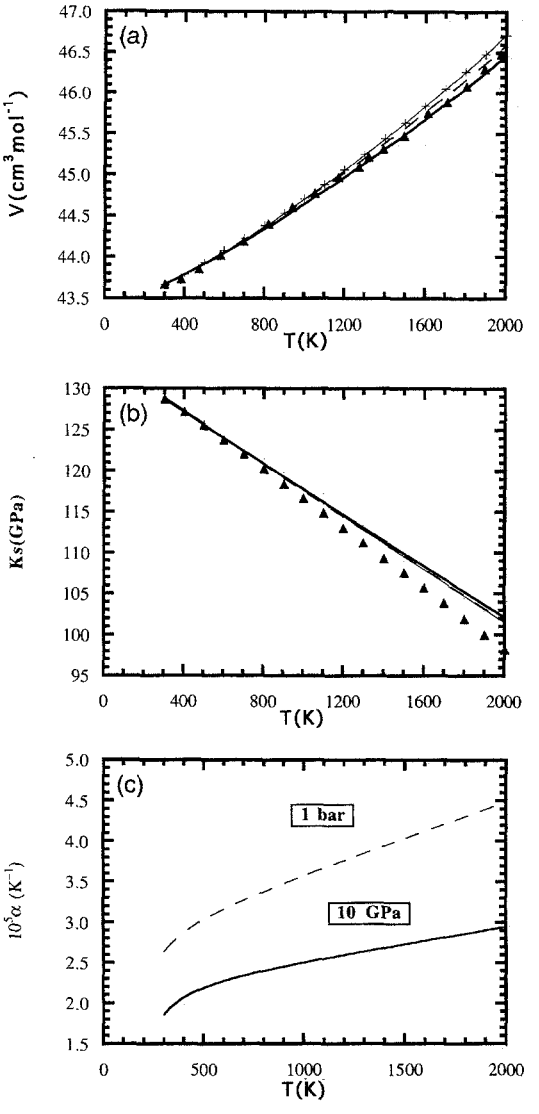

Fig. 6. Comparison of experimental results and model calculations at 1 bar and high temperature for (a) volume, (b) adiabatic incompressibility. Crosses, experimental data of Kajioshi (1986); solid triangles, experimental data from Bouhifd et al. (1996) for volumes and Isaak et al. (1989) for K_S. Thick solid line, INS model; thin solid line, ED model; dashed line, EK model. (c) INS-model calculations of the thermal expansion coefficient of forsterite at 0 GPa (dashed line) and 10 GPa (solid line).

information, match the unpublished experimental data of Kajioshi (1986) and Bouhifd et al. (1996) reasonably well up to 1300 K. Above this temperature, the INS model is more consistent with the data of Bouhifd et al. (personal communication, 1995). At

very high temperatures, the agreement with the measurements might however be rather fortuitous because uncertainties due to unknown parameters such as q or m become important. For example, if an average value of q equal to 1.5 is used instead of 1, the INS model matches the values given by the Debye model and by Kajioshi (1986) at high temperature. Also, intrinsic anharmonic effects might become important at high temperature and a value of the intrinsic anharmonic parameter m of 2 instead of 0 is enough to bring the spectroscopic values close to the values of the ED model. It should be kept in mind, however, that all these determinations are very close (within less than 1%) and we believe that we now have a very good sense of the very high temperature molar volumes of forsterite. Eventually, a last test is given by the 1-bar high-temperature measurements of the adiabatic incompressibility of Isaak et al. (1989). The results are shown in Fig. 6(b). All three models overestimate K_S at high temperature by about 4% at 2000 K which implies imprecisions of about 15% on the temperature derivative of K_S. This might be a direct evidence of intrinsic anharmonic effects in Eq. (5) and Eq. (8) which have not been taken into account in the different density of state-based models. Such uncertainties, small in some sense, are still big in terms of geophysical applications (compare for example with the differences in K_S and density between pyrolitic and piclogitic models of the upper mantle given in Ita and Stixrude (1992).

Table 7
Gibbs free energy (kJ mol^{-1}), volume (cm^3 mol^{-1}) and entropy (J mol^{-1} K^{-1}) of forsterite calculated with the INS model are given at various P, T conditions, encompassing the stability field

P (GPa)	T (K)				
	300	700	1100	1500	1900
0	−2210	−2270	−2370	−2500	−2650
	43.67	44.19	44.80	45.49	46.26
	95.3	216.0	294.2	351.7	397.7
5	−1990	−2050	−2150	−2280	−2430
	42.13	42.54	43.03	43.57	44.15
	90.6	209.6	286.9	343.6	388.6
10	−1780	−1840	−1940	−2070	−2210
	40.85	41.19	41.60	42.04	42.51
	87.0	204.6	281.3	324.7	380.7
15	−1580	−1640	−1740	−1860	−2000
	39.76	40.05	40.39	40.77	41.16
	84.0	200.5	276.7	319.8	376.5

Table 8
Thermoelastic parameters derived from the INS model compared with the results of previous studies

	INS-model	Gillet et al. (1991)	Isaak et al. (1989)
$10^5\alpha_0$	2.7	2.77	
$10^8\alpha_1$	0.9	0.97	
α_2	−0.31	−0.32	
$(\partial K/\partial T)_P$	−0.02	−0.02	−0.023
δ_T	5.5		5.94

$V_0 = 43.67$ cm^3 mol^{-1}, $K_0 = 127.4$ GPa (Isaak et al., 1989), $K'_0 = 4.8$ Graham and Barsch (1969).
$\alpha = \alpha_0 + \alpha_1 T + \alpha_2 / T^2$.
Anderson–Grüneisen parameter δ_T given at 300 K and 1 bar. Average values of δ_T over the P–T field 0–20 GPa, 300–2000 K, given by the INS model is 4.8.

Although the INS-model of forsterite is still imperfect, it is consistent with all the macroscopic measurements made on forsterite, including the P–V–T measurements of this study, as shown above. The discrepancies are at most 4% for the values of K_S at 2000 K. Therefore, we propose a set of self consistent thermodynamic parameters completely derived from the physically sound INS-model and which constrains the thermodynamic properties of forsterite within all its stability field. Let us keep in mind that the only input parameters of the INS-model are V_0, K_0, K'_0, and the vibrational spectroscopic data. The interest of such a model is thus obvious for high-pressure phases such as (Mg,Fe)SiO_3 perovskite, where zero-pressure thermal expansion data are extremely limited due to the marginally metastable nature of the material. The results are shown in Tables 7 and 8. In Table 7, volume, entropy and Gibbs free energy of forsterite are given at various P, T conditions, encompassing the stability field. In Table 8, the thermoelastic parameters provided by the model are summarised. Since volumes have been calculated in the P–T field, α and K_T were determined at different pressures by spline fits of the calculated LnV vs T or P. This allowed to calculate the temperature and pressure derivatives of α and K_T as well as the Anderson–Grüneisen parameter $\delta_T = (\partial \ln \alpha / \partial \ln V)_T = (-1/\alpha K_T)(\partial K_T/\partial T)_P$ given in Table 8. The values of α_0, $(\partial\alpha/\partial T)_P$, $(\partial K/\partial T)_P$ are very close to those

from Gillet et al. (1991) and from the experimental measurements of Isaak et al. (1989). The Anderson–Grüneisen parameter is slightly smaller than in the study of Isaak et al. (1989) and is very close to K'_0. Calculations of third derivatives of the volumes with respect to pressure and/or temperature (e.g. $(\partial K'/\partial P)_T$ or $(\partial \delta_T/\partial T)_P$) were not attempted because the model is not precise enough. However, it is clear that $(\partial \alpha/\partial P)_T$ is much larger at high temperature than at ambient temperature (Fig. 6(c)). Obviously, by the third law of thermodynamics, $\alpha = (\partial \alpha/\partial P)_{0K} = 0$ at the zero temperature limit.

6. Conclusions

In this study, we provide experimental measurements of specific volumes of forsterite and San Carlos olivine in-situ at high pressure and high temperature up to 7 GPa and 1300 K. The data at high-pressure and room temperature were discarded because they are affected by quite high levels of non-hydrostatic stresses. The high-temperature data, free of deviatoric stress, were used for the P–V–T measurements. No difference could be evidenced between the thermal pressures of the two compounds and it is has been shown that the parameter αK_T is volume-independent within the volume range investigated in this study for both forsterite and San Carlos olivine. We observed that the quality of the data in San Carlos olivine is not as good as in forsterite. This could be due to minor chemical destabilisation of Fe^{2+} at high temperatures in the cell assembly; this emphasizes the fact that precise P–V–T measurements at high-temperatures are more difficult on iron-bearing silicates than on iron-free phases. The high-pressure high-temperature volumes and coefficient of thermal expansion of forsterite have been successfully computed with three different quasi-harmonic models: a Debye model, a Kieffer model, and a density of state derived from inelastic neutron scattering. No intrinsic anharmonic effects could be evidenced in the equation of state, although systematic differences between computed and measured $(\partial K_S/\partial T)_P$ might be a sign of significant intrinsic anharmonicity. Moreover, it is necessary to take into account intrinsic anharmonicity measured by vibrational spectroscopy in order to compute the constant pressure specific heat and the entropy at high temperatures. The applicability of such a model extended with caution to high-pressure phases for which thermodynamic measurements are impossible or difficult seems to be a promising contribution to a better understanding of the Earth's deep interior.

Acknowledgements

We wish to thank Isabelle Martinez for her help during the X-ray diffraction experiments at Brookhaven, Lars Stixrude for carefully reading and commenting an early version of the manuscript and Orson Anderson for fruitful discussions. Two anonymous referees are acknowledged for their constructive and helpful reviews. François Guyot benefitted from NATO financial support during his sabbatical year at Stony Brook. The high pressure experiments were performed at the NSF Science and Technology Center for High Pressure Research (EAR89-2039) which is located at the Mineral Physics Institute, Department of Earth and Space Sciences, State University of New York, Stony Brook. This contribution is designated as MPI Publ. No. 181.

References

Anderson, O.L., 1984. A universal thermal equation of state. J. Geodyn., 1: 185–214.

Anderson, O.L., 1995. Equations of State of Solids for Geophysics and Ceramic Science. Oxford Monographs on Geology and Geophysics, 31, Oxford University Press, New York, 405 pp.

Anderson, O.L., Isaak, D. and Oda, H., 1992. High-temperature elastic constant data on minerals relevant to geophysics. Rev. Geophys., 30: 57–90.

Bouhifd, M.A., Andrault, D., Fiquet, G. and Richet, P., 1996, Thermal expansion of forserite up to the melting point, geophys. Res. Lett. 23: 1143–1146.

Chopelas, A., 1990. Thermal properties of forsterite at mantle pressures derived from vibrational spectroscopy. Phys. Chem. Minerals, 17: 149–156.

Decker, D.L., 1971. High-pressure equation of state for NaCl, KCl and CsCl. J. Appl. Phys., 42: 3239–3244.

Gillet, Ph., Richet, P., Guyot, F. and Fiquet, G., 1991. High-temperature thermodynamic properties of forsterite. J. Geophys. Res., 96: 11 805–11 816.

Graham, E.K. and Barsch, G.R., 1969. Elastic constants of single-crystal forsterite as a function of temperature and pressure. J. Geophys. Res., 74: 5949–5960.

Gwanmesia, G.D. and Liebermann, R.C., 1992. Polycrystals of high-pressure phases of mantle minerals: hot-pressing and characterization of physical properties. In: Y. Syono and M.H. Manghnani (Editors), High-Pressure Research, Application to Earth and Planetary Sciences. Terra Scientific, Tokyo and American Geophysical Union, Washington, pp. 117–135.

Hofmeister, A.M., Xu, J., Mao, H.K., Bell, P.M. and Hoering, T.C., 1989. Thermodynamics of Fe–Mg olivines at mantle pressure: mid- and far infrared spectroscopy at high pressure. Am. Mineral., 74: 281–306.

Isaak, D.G., 1992. High-temperature elasticity of iron-bearing olivines. J. Geophys. Res., 97: 1871–1885.

Isaak, D.G., Anderson, O.L. and Goto, T., 1989. Elasticity of single-crystal forsterite measured to 1700 K. J. Geophys. Res., 94: 5894–5906.

Ita, J. and Stixrude, L., 1992. Petrology, elasticity and composition of the mantle transition zone. J. Geophys. Res., 97: 6849–6866.

Kajioshi, K., 1986. High temperature equation of state for mantle minerals and their anharmonic properties. M.S. Thesis, Okayama University, Okayama, Japan.

Kieffer, S.W., 1979a. Thermodynamics and lattice vibrations of minerals 1, mineral heat capacities and their relationships to simple lattice vibrational models. Rev. Geophys., 17: 1–19.

Kieffer, S.W., 1979b. Thermodynamics and lattice vibrations of minerals 3, lattice dynamics and an approximation for minerals with application to simple substances and framework silicates. Rev. Geophys., 17: 827–849.

Kieffer, S.W., 1980. Thermodynamics and lattice vibrations of minerals 4, Application to chain and sheet silicates and orthosilicates. Rev. Geophys., 18: 862–886.

Kumazawa, M. and Anderson, O.L., 1969. Elastic moduli, pressure derivatives and temperature derivatives of single-crystal olivine and single-crystal forsterite. J. Geophys. Res., 74: 5961–5972.

Meng, Y., Weidner, D.J., Gwanmesia, G.D., Liebermann, R.C., Vaughan, M.T., Wang, Y., Leinenweber, K., Pacalo, R.E., Yeganeh-Haeri, A. and Zhao, Y., 1993. In-situ high P–T X-ray diffraction studies on the three polymorphs (a, b, g) of Mg_2SiO_4. J. Geophys. Res., 98: 22199–22207.

Ohtani, E., Kumazawa, M., Kato, T. and Irifune, T., 1982. Melting of various silicates at elevated pressures. In: S. Akimoto and M.H. Manghnani (Editors), High-Pressure Research in Geophysics, AEPS 12. Center for Academic Publications Tokyo and D. Reidel Publishing Company Dordrecht, pp. 259–270.

Rao, K.R., Chaplot, S.L., Chowdhury, N., Ghose, S. Hastings, J.M. and Corliss, L.M., 1988. Lattice dynamics and inelastic neutron scattering from forsterite: Phonon dispersion relation, density of states, and specific heat. Phys. Chem. Minerals, 16: 83–97.

Saxena, S.K., Chatterjee, N. and Shen, G. 1993, Thermodynamic data on oxides and silicates, Springer-Verlag, Berlin, pp. 428.

Schwab, R.G. and Küstner, D., 1977. Präzisiongitterkonstantenbestimmung zur Festlegung röntgenographischer Bestimmungkurven für syntetische Olivine der Mischkristallreihe Forsterit-Fayalit. N. Jb. Miner. Mh., H5: 205–215.

Wallace, D.C., 1972. Thermodynamics of Crystals. Wiley and Sons, New-York, 484 pp.

Wang, Y., Weidner, D.J., Liebermann, R.C. and Zhao, Y., 1994. P–V–T equation of state of $(Mg,Fe)SiO_3$ perovskite: constraints on composition of the lower mantle. Phys. Earth Planet. Inter., 83: 13–40.

Weidner, D.J., Vaughan, M.T., Ko, J., Wang, Y., Liu, X., Yeganeh-Haeri, A., Pacalo, R.E. and Zhao, Y., 1992. Characterisation of stress, pressure, and temperature in SAM 85, a DIA type high-pressure apparatus. In: Y. Syono and M.H. Manghnani (Editors), High-Pressure Research, Application to Earth and Planetary Sciences. Terra Scientific, Tokyo and American Geophysical Union, Washington, pp. 13–17.